Research Article Vol. 30, No. 6 / 14 Mar 2022 / Optics Express 9714
Optics EXPRESS

High-performance temperature and pressure dual-parameter sensor based on a polymer-coated tapered optical fiber

JUNYANG LU,[1,2,3,6] YANG YU,[2,3,6] SHANGPENG QIN,[1,2,3] MINWEI LI,[1,2,3] QIANG BIAN,[4] YANG LU,[5] XIAOYANG HU,[5] JUNBO YANG,[2] ZHOU MENG,[5] AND ZHENRONG ZHANG[1,*]

[1]*Guangxi Key Laboratory of Multimedia Communications and Network Technology, School of Computer, Electronic and Information, Guangxi University, Nanning 530004, China*
[2]*College of Liberal Arts and Sciences, National University of Defense Technology, Changsha 410073, China*
[3]*State Key Laboratory of Transducer Technology, Shanghai Institute of Microsystem and Information Technology, Chinese Academy of Sciences, Shanghai 200050, China*
[4]*Institute for Measurement and Sensor Technology, Technical University Munich, Munich D-80333, Germany*
[5]*College of Meteorology and Oceanography, National University of Defense Technology, Changsha 410073, China*
[6]*These authors contributed equally to this work and should be considered co-first authors*
[*]*zzr76@gxu.edu.cn*

Abstract: Based on the polymer encapsulation method, a compact structure and high-sensitivity temperature and pressure dual parametric sensor was developed in this paper by wrapping an optical microfiber coupler (OMC) in polydimethylsiloxane (PDMS). Benefiting from the stable chemical properties and good optical field control ability of PDMS, the sensor showed good stability and repeatability. The dependence of the sensor sensitivity on wavelength, temperature, and pressure was experimentally investigated. The results showed that the temperature and pressure sensitivity could reach −2.283 nm/°C and 3.301 nm/Mpa in the C-band range. To overcome the cross-sensitivity of sensor temperature and pressure, a sensitivity matrix was established to realize dual-parameter simultaneous demodulation. In addition, the pressure repeatability of the sensor was tested. Based on this, the sensitivity matrix was further calibrated to reduce the error and improve the accuracy of demodulation. Finally, we also designed a protective shell for the sensor to meet the requirements of practical marine applications. Compared with other existing types of optical fiber sensors, this sensor has the advantages of simple fabrication, high sensitivity, and environmental adaptability, and has great potential for application in the field of marine environmental monitoring.

1. Introduction

The temperature and depth of seawater are important basic parameters for human exploration of the ocean, and accurate measurement of these two parameters is essential for marine scientific research [1,2]. At present, almost all ocean monitoring platforms, such as stations, ships, buoys, submersible, and other above-water platforms, are equipped with relevant temperature, salinity, and depth sensors. As a part of sensing, the sensor is a crucial core device in the field of marine exploration, which can be divided into electrical sensors and optical fiber sensors. Traditionally, the commonly used method for measuring temperature and pressure in seawater is the conductivity-temperature-depth (CTD) system. As an electrical equipment, it often suffers from problems of high price, electromagnetic interference and high requirement for water tightness. On the contrast, optical method, especially the optical fiber sensor shows prominent advantages of low cost, multi-parameter sensing, electromagnetic immunity and no requirement

#452355 https://doi.org/10.1364/OE.452355
Journal © 2022 Received 27 Dec 2021; revised 10 Feb 2022; accepted 12 Feb 2022; published 9 Mar 2022

Optics EXPRESS

for water tightness [3]. It can be expected that it will be a meaningful thing to develop an optical fiber sensor used for temperature and pressure simultaneous measurement in seawater for low cost, high accuracy, fast laying and widespread applications in future.

Currently, the optical fiber sensors applied in the field of marine environmental monitoring are numerous, including fiber Bragg grating (FBG) [4,5], surface plasmon resonance (SPR) [6], tapered fiber [7,8], Mach-Zehnder interferometer (MZI) [9,10], etc. Although they perform better than traditional electrical sensors in terms of size, cost, and networking, there are still some key problems to be solved, such as low sensitivity, poor environmental adaptation, and difficulty in synchronous multi-parameter sensing. In addition, Min et al. also highlight the fact that fiber optic sensing technology still needs further improvement in practical applications when facing the harsh environment of the ocean [11]. Therefore, some researchers have proposed that optical fibers can be protected and sensitized by special encapsulation methods. According to the form and material, the specific encapsulation methods can be divided into: protective encapsulation, sensitization encapsulation, temperature compensated encapsulation, etc. Sun *et al.* used polyurethane to protectively encapsulate an exposed fiber grating, making the sensor resilient in harsh environments and extending its life cycle [12]. Jiang *et al.* successfully enhanced the sensor response to temperature by encapsulating an optical microfiber coupler in Teflon capillary filled with refractive index matching liquids [13]. In the field of wearable sensing, encapsulation also plays an equally pivotal role. Owing to the fact that the mechanical properties of optical fibers are not compatible with flexible human skin leading to a limited range of measuring large strains (<1%), Guo *et al.* encapsulated optical fiber gratings into PDMS to fabricate a skin-like flexible optical strain sensor for human activity monitoring [14]. Zhang *et al.* implemented the monitoring of human high-frequency vibration and wrist pulses by encapsulating micro/nanofibers (MNFs) in a thin PDMS layer [15], which provided a protective effect on the MNF and effectively improved its mechanical flexibility. Similar solution with special package design can be applied when using optical fiber sensors in oceanic parameters measurements.

As one of the representatives of tapered optical fiber, the optical microfiber coupler (OMC) is a basic passive optical device with the advantages of large-scale evanescent field transmission characteristics, strong optical confinement ability, small loss, and small size, which has been widely applied in optical fiber communication, optical fiber sensing, and other fields [16–19]. In particular, it has shown good application potential in the field of physical parameter sensing and monitoring in recent years. In 2019, Yu *et al.* conducted studies on the three-parameter sensing characteristics of seawater temperature, salinity, and depth based on OMC and achieved good results [1,20,21]. However, the poor stability, short life cycle, and multi-parameter cross-sensitivity problems faced by the sensor remain unsolved. The major reason for these problems is that OMC has a large evanescent field in seawater, which is extremely sensitive to environmental interference and pollution, resulting in unpredictable changes in the guidance signals. To solve these problems, the OMC evanescent field must be properly controlled.

Due to stable chemical properties, low refractive index, high thermal-optical coefficient, high flexibility, and good bio-compatibility, PDMS is widely used in the sensing field [22–24]**.** It can effectively manage the evanescent field, and provide adequate protection to the optical fiber as well. Most importantly, it is well suited as a temperature and pressure sensing medium, which can significantly improve the sensitivity of the sensor. Therefore, combined with Faraday rotating mirrors (FRMs), a high-sensitivity reflection optical microfiber coupler interferometer (OMCI) sensor using PDMS as the sensing medium and OMC as the carrier is demonstrate, by which typical sensitivities of −2.283 nm/°C and 3.301 nm/Mpa are obtained, respectively. Based on these sensitivities, a sensitivity matrix can be established and the matrix can be solved to achieve simultaneous temperature and pressure measurements. By comparing the results with those measured by CTD, the average errors of the sensor for temperature and pressure measurement

Optics EXPRESS

were 0.67% and 4.43%, respectively. Compared with the conventional transmission OMC, the reflection OMCI enhanced the compactness and integration of the device and solved the problem of redundant OMC output ports. Meanwhile, the light would be transmitted twice in the OMC coupling region under the action of the FRM, forming a quasi-resonant structure to improve the sensitivity of the sensor. Overall, our proposed sensor has the advantages of compactness, high sensitivity, stability, and environmental adaptability, providing a new method for simultaneous measurement of seawater temperature and pressure.

2. Structure and sensing principle

In this paper, the schematic structure of OMCI for simultaneous seawater temperature and pressure measurement is shown in Fig. 1. This structure is constructed by connecting FRMs to the two ports of the microfiber coupler, respectively. OMC, as the core part of the device, is packaged in PDMS, including two tapered transition regions and a uniform waist region.

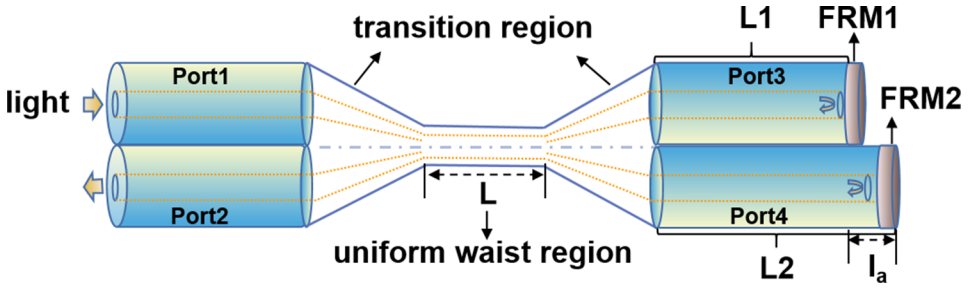

Fig. 1. Schematic diagram of OMCI.

When the input light with total power P1 is injected from Port1, it will be divided into Port3 and Port4 after the first coupling, and then re-enter the OMC under the reflection of FRM for the second coupling and superposition interference. Because of the sensitization effect of PDMS, the encapsulated OMCI is very sensitive to temperature and pressure changes. The response signal can be obtained by monitoring Port2. According to the coupling theory, the output optical power of Port3 and Port4 can be expressed as [1]:

$$P_3 = P_1 \cos^2(CL) \tag{1}$$

$$P_4 = P_1 \sin^2(CL) \tag{2}$$

where C is the coupling coefficient and L is the coupling length. Theoretically, the uniform waist region and the partially tapered transition region of the OMC both play an important role in the coupling characteristics of the whole device. In fact, the contribution generated by the transition regions is much lower than that of the uniform waist area due to the large geometric size difference [25]. Therefore, we can neglect the contribution of the conical transition zone and analyze the contribution of the uniform waist zone. Under strong coupling, the coupling coefficient can be expressed as [1,2]:

$$C(\lambda, n_2, n_3) = \frac{3\pi\lambda}{32 n_2 r^2} \times \frac{1}{(1 + 1/V)^2} \tag{3}$$

where $V = [(2\pi r)/\lambda](n_2^2 - n_3^2)^{1/2}$ represents the normalized power, λ represents the wavelength of the incident light, r is the radius of the microfiber at the waist region, n_2 and n_3 are the refractive indices of the fiber cladding and PDMS, respectively. Assuming that the reflection efficiency of

Optics EXPRESS

the FRM is 100%, the output optical power of Port2 according to the two-beam coherent light interference theory can be expressed as follows [20,21]:

$$P_2 = P_3 \sin^2(CL) + P_4 \cos^2(CL) + 2\sqrt{P_3 \sin^2(CL) P_4 \cos^2(CL)} \cos\varphi \tag{4}$$

After simplification, it can be expressed as:

$$P_2 = 2P_1 \cos^2(CL) \sin^2(CL)(1 + \cos\varphi) \tag{5}$$

In the Eq. (5), $\varphi = 2\pi n_2 l_a/\lambda$ is the phase difference of the interference, and $l_a = L_2 - L_1$ represents the arm difference of the interferometer. It should be noted that different arm differences will produce the phenomenon of change of interference fringe spacing in the envelope of each interference wave peak or interference wave valley, and l_a should be controlled within 5–30 mm to shape its envelope [20].

It can be seen from Eqs. (3) and (4) that the output power of port2 depends on the refractive index n_3 of PDMS and the structural parameters (r, L, n_2) of OMC. Considering that the diameter of the uniform waist region is on the order of micrometers or even nanometers, most of the energy in this region will be propagated in the sensing medium in the form of evanescent fields, so it will be very sensitive to changes in the surrounding environment. When the external temperature changes, the relevant parameters of the sensor change (r, L, n_2, n_3) due to the thermo-optical and thermal expansion effects of the PDMS, resulting in wavelength drift of the output spectrum. Therefore, the temperature sensitivity of the device can be calculated based on the drift of a particular interference peak and valley with increasing temperature. The temperature sensitivity can be expressed as:

$$S_T = \frac{d\lambda}{dT} = -\frac{\partial\lambda}{\partial\varphi}\left(\frac{\partial\varphi}{\partial n_3}\cdot\frac{dn_3}{dT} + \frac{\partial\varphi}{\partial n_2}\cdot\frac{dn_2}{dT} + \frac{\partial\varphi}{\partial L}\cdot\frac{dL}{dT} + \frac{\partial\varphi}{\partial r}\cdot\frac{dr}{dT}\right). \tag{6}$$

Since the thermal-optical (-4.5×10^{-4} /°C) and thermal-expansion coefficients (9.6×10^{-4}/°C) of PDMS are much higher than silica, it is conceivable that the temperature sensitivity of the device will be greatly enhanced relative to the all-silica structure, according to Eq. (6).

Similarly, when the external pressure changes, the characteristic wavelength of the output spectrum will also drift due to the elastic effect of PDMS. The pressure sensitivity can be expressed as:

$$S_P = \frac{d\lambda}{dP} = -\frac{\partial\lambda}{\partial\varphi}\left(\frac{\partial\varphi}{\partial n_3}\cdot\frac{dn_3}{dP} + \frac{\partial\varphi}{\partial n_2}\cdot\frac{dn_2}{dP} + \frac{\partial\varphi}{\partial L}\cdot\frac{dL}{dP} + \frac{\partial\varphi}{\partial r}\cdot\frac{dr}{dP}\right). \tag{7}$$

Therefore, the temperature and pressure can be measured by tracking the shift of the characteristic wavelengths (peaks or valleys) in the output spectrum with proper calibration.

3. Experiment and results

3.1. Fabrication of the sensor

The fabrication process of the proposed OMCI sensor involves the following steps.

Firstly, two conventional single-mode fibers (SMF-28e+) were taken, and stripped of about 3 cm of the coating at the same location, and then screwed twice to fix them on the OMC drawing device as shown in Fig. 2. After that, the structural parameters of the sample were entered on the PC terminal, and the device started to slowly stretch the fiber to obtain a four-port coupler.

Then, the four-port OMC is removed from the device and fixed in the groove with a protective cover. One purpose is to prevent dust in the air from attracting the coupling area and causing loss to the sample. Another purpose is to facilitate subsequent packaging operations.

Optics EXPRESS

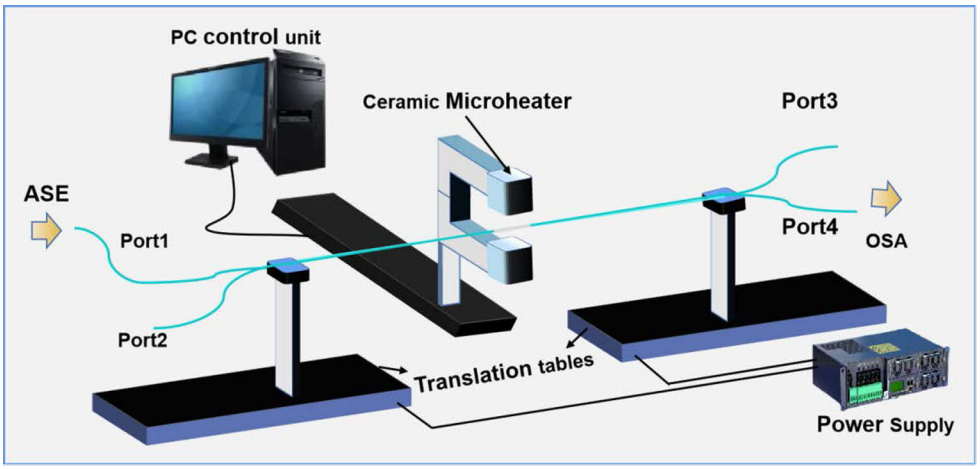

Fig. 2. Schematic of experimental setup for fabricating OMC.

Immediately afterwards, a quantity of PDMS liquid was prepared, which was made by mixing Reagent A (primary agent, Hamld) and Reagent B (curing agent) in a 10:1 ratio [24]. Before packaging the samples, the PDMS liquid was vacuumed to remove air bubbles. Then the groove was filled with an appropriate amount of PDMS liquid using a syringe to completely submerge the OMC, as shown in Fig. 3(a). Finally, the whole was put into a high-temperature oven at 60 °C for 2 hours to cure.

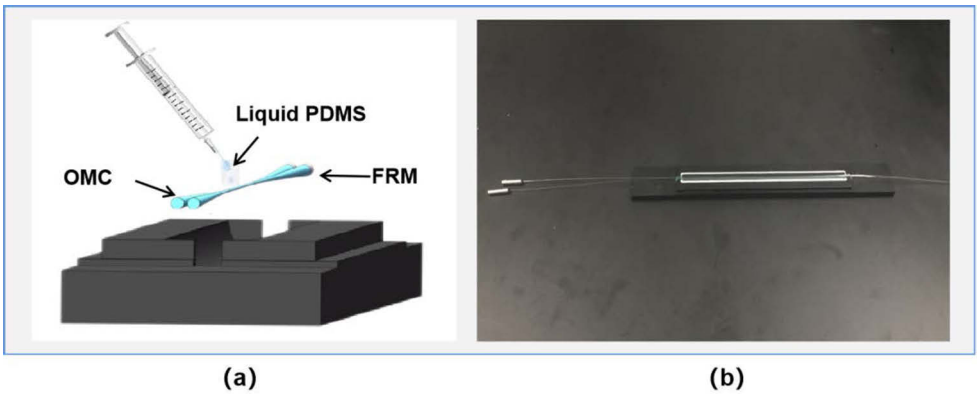

Fig. 3. (a) Schematic diagram of packaging bare OMC in PDMS; (b) Photograph of the sensor.

After removing the cured sample from the temperature chamber, the FRMs were fused to the two output ports of the OMC to obtain the reflection OMCI.

Finally, an OMCI sample was successfully fabricated, as shown in Fig. 3(b). The OMC uniform waist radius (r) was 3 μm, and the waist coupling length (L) was 8 mm, and the arm difference of the interferometer was controlled as $l_a \approx 7$ mm.

3.2. *Experiments of temperature and pressure sensing*

Based on the fabrication of the above structure, temperature sensing experiment can be performed. The schematic diagram of the experimental system is shown in Fig. 4(a), which contained an Amplified Spontaneous Emission source (ASE), an Optical Spectrum Analyzer (OSA, Yokogawa,

Optics EXPRESS

Japan, AQ6370D), a temperature-controlled water tank (KQ2200DE) with seawater samples, and a conductivity-temperature meter (WS-A1521). The sensor Port1 in the system was connected to ASE with an emission wavelength of 1528 nm~1603 nm, and Port2 was connected to OSA for receiving optical signals. The temperature measuring experimental setup is shown in Fig. 4(b), where the seawater sample in the water tank was mainly configured by pure water and Nacl about 2 liters. Before conducting the experiment, the initial temperature and salinity measured by conductivity meter were 21.5 °C and 17.3 ‰, respectively. The resolution of the OSA was set to be 0.02 nm.

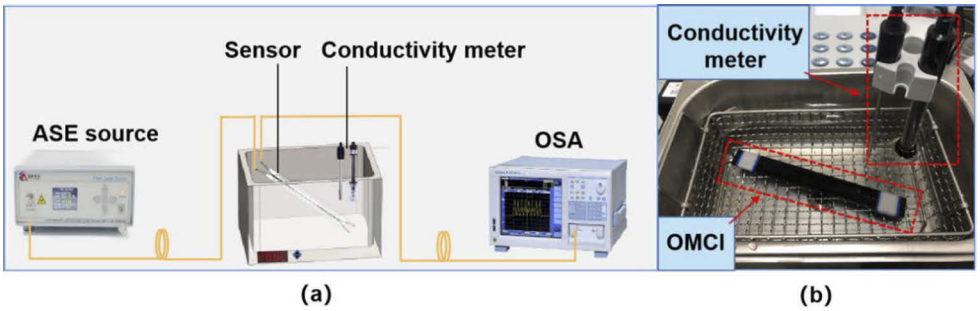

Fig. 4. (a) The schematic diagram of the temperature experiment system; (b) The temperature measuring experimental setup.

In order to avoid errors caused by uneven heating of seawater temperature during the experiment, we carried out the temperature response test with the natural cooling method. After placing the prepared OMCI samples into the temperature-controlled water tank, the seawater samples were slowly heated to 32 °C and remained there for 15 minutes. Then the heating equipment was turned off to start recording the output spectra corresponding to different temperatures. Meanwhile, the temperature and salinity of the seawater sample were measured by a conductivity meter in real-time. Figure 5(a) showed the interference spectra of the sensor in the wavelength range of 1520 nm~1620 nm observed on the OSA when the seawater temperature was increased from 21.5 °C to 28 °C. It can be observed that the interference spectrum has a regular shape and the extinction ratio (the difference between wave peak and dip) reached about 15 dBm. The interference spectrum shifted significantly to the short-wave direction with the increase of seawater temperature. For the output spectra at different temperatures, we used the "Peak Search" and "Bottom Search" functions of OSA to find these dips or peaks and record them. By tracking typical sensing dips, such as dip1, dip2, dip3, and dip4, relationships between the wavelength of sensing dips and the pressure can be obtained, as shown in Fig. 4(b), indicating the sensing sensitivities of −1.599 nm/°C, - 1.771 nm/°C, −2.007 nm/°C and −2.283 nm/°C, respectively.

The pressure response of the same sensor was tested using the experimental schematic shown in Fig. 6(a), in which the sensor was removed from the above water tank and placed in a pressure tank filled with seawater. Figure 6(b) depicts the pressure measuring experimental setup.

The pressure response of the sensor was measured by varying the water pressure to simulate water depth in this paper. The sensor's interference spectrum is shown in Fig. 7(a) as the water pressure increases from 0 Mpa to 3 Mpa at room temperature (21.5 °C). It can be concluded from the figure that the sensor response to pressure has good linearity. Similarly, the wavelengths corresponding to three dips at different pressures were recorded by the "valley search" function of OSA while the output spectrum was shifted to the long wavelength direction. The pressure sensitivities of dip1, dip2, and dip3 are plotted in Fig. 7(b), with pressure sensitivities of 2.63 nm/Mpa, 2.927 nm/Mpa, and 3.301 nm/Mpa, respectively. Among them, the pressure sensitivity of dip3 is about 20 times higher than the pressure sensitivity (169 pm/Mpa) of

Optics EXPRESS

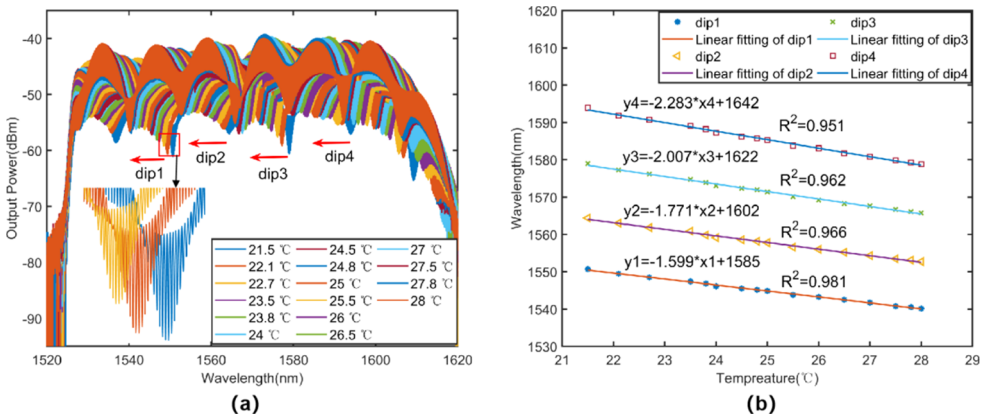

Fig. 5. (a) Interference spectra at different temperatures; (b) Relationships between the dip wavelengths and the temperatures.

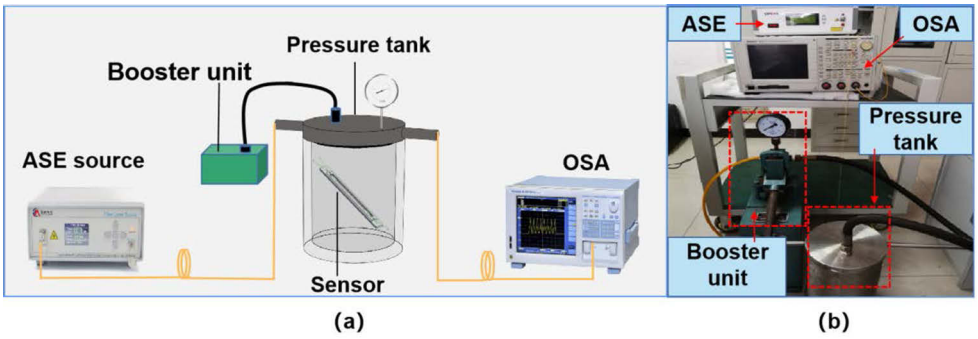

Fig. 6. (a) The schematic diagram of the pressure experiment system; (b) the pressure measuring experimental setup.

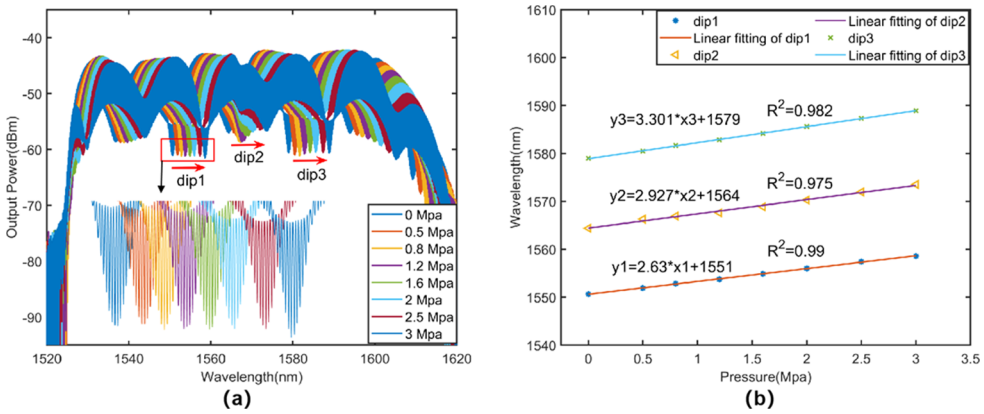

Fig. 7. (a) Interference spectra at different pressures; (b) Relationships between the dip wavelengths and the pressures.

Optics EXPRESS

bare OMC [1]. In fact, since optical microfiber coupler is wavelength dependent in sensing applications, i.e., they exhibit different sensitivities at different wavelengths, the larger the wavelength, the higher the sensitivity.

3.3. Two-parameter demodulation

According to the above measurements, the sensor has an excellent response to seawater temperature and pressure variations. However, when the temperature and pressure change simultaneously, the sensor has to deal with the problem of interaction between the two parameters. Therefore, how to demodulate the individual parameters from the output signal is also a key problem that needs to be solved for optical fiber sensors. Considering our sensor meets the requirement of good linearity, we can construct a sensitivity matrix by collecting the sensitivity at two different wavelengths to measure temperature and pressure simultaneously. The specific form can be expressed as follows.

$$\begin{bmatrix} \Delta\lambda_{dip1} \\ \Delta\lambda_{dip3} \end{bmatrix} = \begin{bmatrix} -1.599nm/^{\circ}\mathrm{C} & 2.63nm/Mpa \\ -2.007nm/^{\circ}\mathrm{C} & 3.301nm/Mpa \end{bmatrix} \begin{bmatrix} \Delta T \\ \Delta P \end{bmatrix} \tag{8}$$

where $\Delta\lambda_{dip1}$ and $\Delta\lambda_{dip3}$ represent the shifts of two different wavelengths, ΔT and ΔP represent the temperature and pressure variations, respectively.

To further validate and demodulate the sensitivity matrix, we chose a sample with a temperature of 21.5 °C and a pressure of 0 MPa as the standard sample to calibrate the system. After calibrating the initial wavelengths of dip1 and dip3, Eq. (8) can be evolved into the following format.

$$\begin{bmatrix} \lambda_{dip1} - 1550.6 \\ \lambda_{dip3} - 1579 \end{bmatrix} = \begin{bmatrix} -1.599nm/^{\circ}\mathrm{C} & 2.63nm/Mpa \\ -2.007nm/^{\circ}\mathrm{C} & 3.301nm/Mpa \end{bmatrix} \begin{bmatrix} T - 21.5 \\ P - 0 \end{bmatrix} \tag{9}$$

where λ_{dip1} and λ_{dip3} are the final wavelengths after dip1 and dip3 shifts, T and P are the current seawater temperature and pressure, respectively.

Table 1. Demodulation results of temperature and pressure

	Temperature (°C)			Pressure (Mpa)		
NO.	OMCI	Reference	Error	OMCI	Reference	Error
Test1	24.65	25	1.4%	1.42	1.5	5.33%
Test2	23.66	23.5	0.68%	2.27	2.5	9.2%
Test3	29.01	29.3	0.98%	3.55	4	11.25%
Test4	25.35	25.5	0.58%	3.14	3.1	1.29%
Test5	20.94	20.5	2.14%	5.21	5	4.2%

With the fabricated sample, we conducted several tests at random temperatures and pressures. By observing the position of dip1 and dip3 in the interference spectra under different conditions to judge the feasibility of the method, as shown in Fig. 8. In view of this, we conducted five tests again based on the pointer pressure gauge and temperature meter as a reference, and the final results of the demodulation are shown in Table 1. The results showed that the demodulation of temperature was excellent, with an average absolute error of only 1.12%. However, the average absolute error in pressure reached 6.22%. There are two potential reasons for the large error in the pressure demodulation results. One is that the pressure sensitivity calculation is inaccurate due to possible slight changes in temperature during the pressure experiment. Another is probably caused by the relatively low accuracy of the pointer pressure meter.

Optics EXPRESS

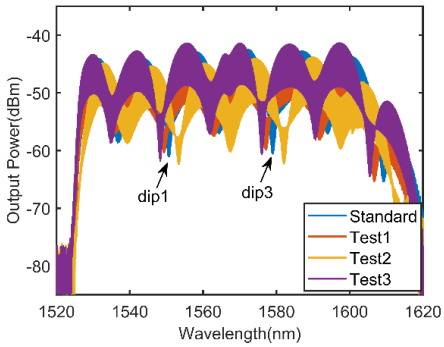

Fig. 8. Random testing under arbitrary conditions.

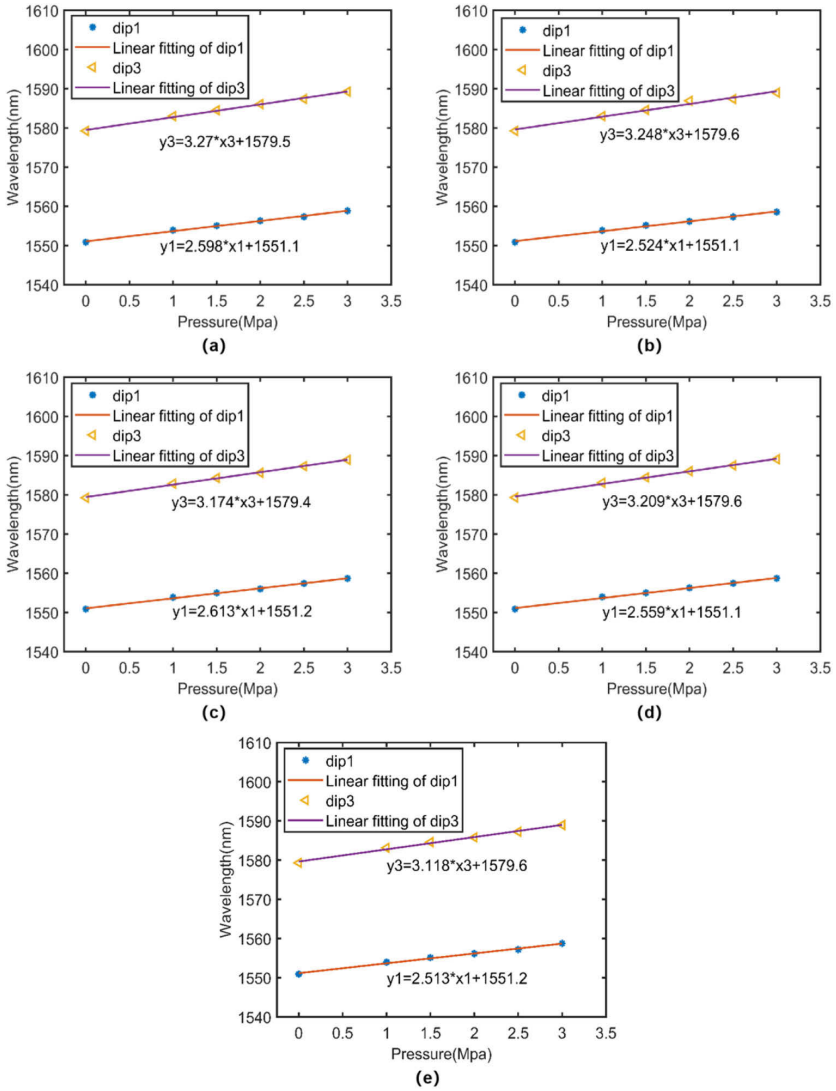

Fig. 9. (a)~(e). Repeatability test of dip1 and dip3 in pressure sensing.

Optics EXPRESS

3.4. Repeatability test

Repeatability is one of the most important indicators for evaluating the performance of sensors, which is closely related to the stability of sensors. Therefore, the repeatability of the sensor is also investigated in this paper. From the above experimental results, the sensor response to temperature and pressure exhibited good linearity, so the repeatability of the sensor can be researched by tracking typical characteristic wavelengths. Considering the length of the article, only the pressure repeatability of the sensor has been tested. Under the same measurement conditions, five pressure increase and decrease tests were performed for a short period of time to track dip1 and dip3 simultaneously, and complete graphs of sensor repeatability were obtained, as shown in Fig. 9(a)~(e). The results showed good repeatability of the pressure sensitivity with an average error of less than 2.9%. In addition, it can be found from the different experimental results that the characteristic wavelengths at the same pressure are not exactly equal, which confirmed the existence of some errors in the experimental results.

4. Discussion

According to the experimental results in Table 1, the problem of cross-sensitivity of the sensor to temperature and pressure was successfully solved by constructing the sensitivity matrix. However, it should be noted that the sensitivity matrix as the coefficients of the binary first-order equation is the key to the accuracy of the demodulation results. The demodulation results could be affected if there is a certain measurement error in the sensitivity matrix. In view of this, we concluded two implementable solutions for reducing the error of experiment. One is to improve the measurement accuracy of the experimental equipment. The other is to conduct multiple tests on the same sample, record the results of each test, and then take the average value to improve the accuracy of the results.

Based on the above pressure repeatability experiments, we validated the second scheme. The results of the six pressure experiments described above are averaged and then used to update the sensitivity matrix, as shown in the following equation.

$$\begin{bmatrix} \lambda_{dip1} - 1550.6 \\ \lambda_{dip3} - 1579 \end{bmatrix} = \begin{bmatrix} -1.599nm/^{\circ}\mathrm{C} & 2.565nm/Mpa \\ -2.007nm/^{\circ}\mathrm{C} & 3.23nm/Mpa \end{bmatrix} \begin{bmatrix} T - 21.5 \\ P - 0 \end{bmatrix} \tag{10}$$

The final demodulation results are shown in Table 2, and it can be seen that the demodulation results for pressure in particular have improved significantly compared to the previous results. It can be seen that the repeatability experiment is beneficial in improving the accuracy of the measurement data and reducing the random errors. In the future actual monitoring process of marine environmental parameters, we can achieve further convergence of the sensitivity matrix by conducting more tests on the sensors based on this method, and then establishing a standard database for the PC software to invoke.

Table 2. Demodulation results of temperature and pressure after sensitivity matrix optimization

	Temperature (°C)			Pressure (Mpa)		
NO.	OMCI	Reference	Deviation	OMCI	Reference	Deviation
Test1	24.75	25	1%	1.45	1.5	3.33%
Test2	23.6	23.5	0.42%	2.31	2.5	7.6%
Test3	29.21	29.3	0.31%	3.76	4	6%
Test4	25.35	25.5	0.58%	3.2	3.1	3.22%
Test5	20.72	20.5	1.07%	5.1	5	2%

Optics EXPRESS

To meet the actual application requirements of the ocean, PDMS protection alone is not enough. The composition of seawater is quite complicated, including a large amount of sediment and microorganisms. Therefore, we designed a protective shell, as shown in Fig. 10. The whole shell is made of titanium alloy material, which has the ability to resist pressure in the deep sea, and the surface is also treated with anti-corrosion. It is a cylindrical symmetrical structure with four water inlet holes. The four inlet holes are composed of a filter and a seawater purification cartridge, which are used to block sediment and contaminants in seawater. With the protection of the shell, the performance of the sensor can be further improved and its service life can be extended as well. Overall, the design of this shell is expected to enable the sensor to be put into practical applications.

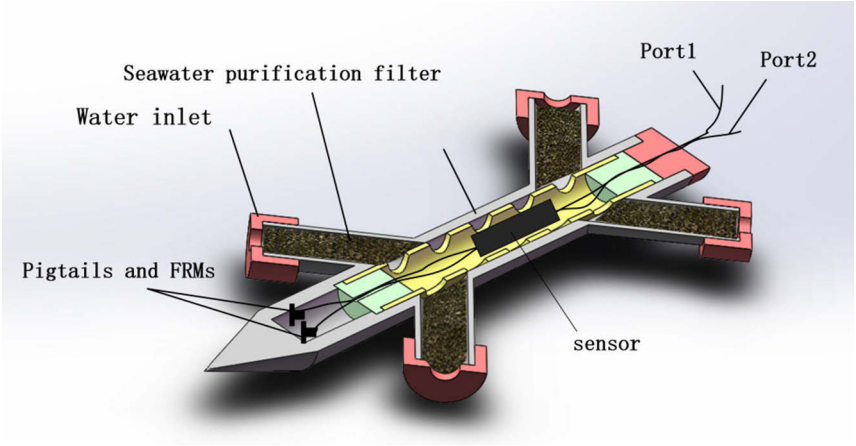

Fig. 10. The schematic diagram of OMCI's protective shell.

In addition, it can be found that the output spectrum of Port2 is related to the structural parameters (*r, L*) of the OMC apart from the refractive index n_3 of PDMS according to Eqs. (3) and (4). Relevant studies have verified that different sensitivities can be obtained by changing the structural parameters of the OMC. For example, higher sensitivity can be obtained by changing the coupling radius. The coupling length L has a relatively small effect on the sensitivity, but it changes the number of characteristic wavelengths [20]. Moreover, the encapsulation thickness of the material also affects the response capability of the sensor. In 2016, Sun *et al.* demonstrated a temperature and humidity sensor with Silica Gel coated OMC and analyzed the effect of coating thickness on the sensor performance. Experimental results show that the sensitivity of the sensor can actually be modulated by varying the package thickness [26]. Therefore, we can optimize the sensitivity of the sensor by tuning the structural parameters of the OMC and the package thickness of the PDMS to obtain sensors with better performance. It is worth noting that the interference arm of the sensor can be further expanded in the future, such as integration with temperature-sensitive and salt-sensitive materials. When the sensing parameters change, the interferometric arm difference can be used to change the interference fringe spacing to achieve multi-parameter sensing or parameter compensation.

We also summarized the performance of our sensor compared with temperature and pressure sensors previously reported by other researchers, as shown in Table 3. Compared with other works, the sensor demonstrated in this paper successfully achieves simultaneous measurement of seawater temperature and pressure based on the dual-wavelength demodulation method. In contrast, most of the other types of sensors can only measure each parametric quantity separately. It can be observed from the table that Zhao *et al.* developed an SPR fiber optic sensor with temperature and pressure sensitivities of −1.802 nm/°C and 2.838 nm/Mpa, respectively. The

Optics EXPRESS

response capability of this sensor is comparable to that of our proposed sensor, but it suffers from the problems of complex process fabrication and high cost. On the contrary, the sensor we demonstrated has obvious features such as low cost, easy fabrication, and good stability. In addition, Arnaldo et al. developed a FBG sensor based on a single-layer polymer diaphragm for simultaneous pressure and temperature measurements [28,29]. The FBG response is analyzed through a transient model for heat conduction and the pressure is estimated with the diaphragm and FBG strain, where the frequency difference between temperature and pressure variations were used to decouple both variables. The results showed a low error of about 5% for both pressure and temperature. It is believed that the application is also a good method in the marine field.

Table 3. Comparison of properties of temperature and pressure sensor reported in other literature.

Sensor structure	Temperature sensitivity	Pressure sensitivity	Sensitivity matrix establishing	Demodulation	Reference
OMC-saganc	248.2 pm/°C	122.6 pm/Mpa	yes	no	[27]
FBG	29.87 pm/°C	1.611 nm/Mpa	no	no	[3]
Fabry–Perot	6.950 nm/°C	0.15 nm/Mpa	no	no	[28]
SPR	−1.802 nm/°C	2.838 nm/Mpa	yes	yes	[6]
FBG	\	\	no	no	[29,30]
Packaged OMCI	−2.283 nm/°C	3.346 nm/Mpa	yes	yes	This work

5. Conclusion

In this paper, a PDMS packaged OMCI sensor was designed and developed for dual parameter detection of temperature and pressure in seawater. The theoretical analysis and experimental validation were successfully performed. The experimental results showed that PDMS could control the swift field of OMC well, which effectively improved the robustness and sensitivity of the sensor. By tracking the shift of the characteristic wavelength, the temperature and pressure sensitivities in the C-band range reached −2.283 nm/°C and 3.301 nm/Mpa. Meanwhile, the simultaneous measurement of seawater temperature and pressure was achieved by constructing a sensitivity matrix using the dual-wavelength demodulation method. In addition, the repeatability of the sensor was well verified. In order to meet the complex environment of marine applications, we had also designed a special protective shell in this paper. In the future, it is expected that the sensor can be further optimized to obtain better performance sensors. In general, the sensor demonstrated in this paper has the advantages of compact structure, easy fabrication, high sensitivity, good environmental adaptability, and strong optimization, which can have broad application prospects in the field of ocean exploration.

Funding. National Natural Science Foundation of China (61775238, 61805278, 61661004); Guangxi Key Research and Development Program (Guangxi Science AB1850043); Guangdong Guangxi Joint Science Key Foundation (2021GXNSFDA076001); State Key Laboratory of Transducer Technology of China (SKT2001).

Acknowledgments. The authors would like to thank the support of the laboratory and university.

Disclosures. The authors declare no conflicts of interest.

Data availability. No data were generated or analyzed in the presented research

References

1. Y. Yu, Q. Bian, Y. Lu, X. Zhang, J. Yang, and L. Liang, "High Sensitivity All Optical Fiber Conductivity-Temperature-Depth (CTD) Sensing Based on an Optical Microfiber Coupler (OMC)," J. Lightwave Technol. **37**(11), 2739–2747 (2019).
2. S. Wang, H. Yang, Y. Liao, X. Wang, and J. Wang, "High-sensitivity salinity and temperature sensing in seawater based on a microfiber directional coupler," IEEE J. Quantum Electron. **51**(5), 1–9 (2015).

Optics EXPRESS

3. L. Men, P. Lu, and Q. Chen, "A multiplexed fiber Bragg grating sensor for simultaneous salinity and temperature measurement," J Appl Phys **103**(5), 053107 (2008).
4. L. Wang, Y. Wang, J. Wang, and F. Li, "A high spatial resolution FBG sensor array for measuring ocean temperature and depth," Photonic Sens **10**(1), 57–66 (2020).
5. D. A. Pereira, O. Frazao, and J. L. Santos, "Fiber Bragg grating sensing system for simultaneous measurement of salinity and temperature," Opt Eng. **43**(2), 299–304 (2004).
6. Y. Zhao, Q. L. Wu, and Y. N. Zhang, "Simultaneous measurement of salinity, temperature and pressure in seawater using optical fiber SPR sensor," Measurement **148**, 106792 (2019).
7. R. Yang, Y.-S. Yu, Y. Xue, C. Chen, C. Wang, F. Zhu, B.-L. Zhang, Q.-D. Chen, and H.-B. Sun, "A highly sensitive temperature sensor based on a liquid-sealed S-tapered fiber," IEEE Photonics Technol. Lett. **25**(9), 829–832 (2013).
8. S. Wang, Y. Liao, H. Yang, X. Wang, and J. Wang, "Modeling seawater salinity and temperature sensing based on directional coupler assembled by polyimide-coated micro/nanofibers," Appl. Opt. **54**(34), 10283–10289 (2015).
9. C. Mao, B. Huang, Y. Wang, Y. J. Huang, L. F. Zhang, Y. Shao, and Y. P. Wang, "High-sensitivity gas pressure sensor based on hollow-core photonic bandgap fiber Mach-Zehnder interferometer," Opt. Express **26**(23), 30108–30115 (2018).
10. H. Luo, Q. Sun, Z. Xu, D. Liu, and L. Zhang, "Simultaneous measurement of refractive index and temperature using multimode microfiber-based dual Mach–Zehnder interferometer," Opt. Lett. **39**(13), 4049–4052 (2014).
11. R. Min, Z. Liu, L. Pereira, C. Yang, Q. Sui, and C. Marques, "Optical fiber sensing for marine environment and marine structural health monitoring: A review," Opt Laser Technol. **140**(6903), 107082 (2021).
12. W. Sun, L. Jia, Z. Wang, Z. Jia, and O. Science, "Optical fiber sensor encapsulated by polyurethane," Optik **165**, 124–131 (2018).
13. Y. Jiang, Z. Fang, Y. Du, E. Lewis, G. Farrell, and P. Wang, "Highly sensitive temperature sensor using packaged optical microfiber coupler filled with liquids," Opt. Express **26**(1), 356–366 (2018).
14. J. Guo, K. Zhao, B. Zhou, W. Ning, K. Jiang, C. Yang, L. Kong, and Q. Dai, "Wearable and Skin-Mountable Fiber-Optic Strain Sensors Interrogated by a Free-Running, Dual-Comb Fiber Laser," Adv. Opt. Mater. **7**(12), 1900086 (2019).
15. L. Zhang, J. Pan, Z. Zhang, H. Wu, N. Yao, D. Cai, Y. Xu, J. Zhang, G. Sun, and L. Wang, "Ultrasensitive skin-like wearable optical sensors based on glass micro/nanofibers," Opto-Electron. Adv. **3**, 19002201 (2020).
16. H. Ahmad and A. Jasim, "Fabrication and characterization of 2× 2 microfiber coupler for generating two output stable multiwavelength fiber lasers," J. Lightwave Technol. **35**(19), 4227–4233 (2017).
17. Y. Jung, G. Brambilla, and D. J. Richardson, "Optical microfiber coupler for broadband single-mode operation," Opt. Express **17**(7), 5273–5278 (2009).
18. W. Zhou, K. Li, Y. Wei, P. Hao, M. Chi, Y. Liu, and Y. Wu, "Ultrasensitive label-free optical microfiber coupler biosensor for detection of cardiac troponin I based on interference turning point effect," Biosens. Bioelectron. **106**, 99–104 (2018).
19. Y. Zhao, Y. Peng, M.-Q. Chen, F. Xia, and R.-J. Tong, "U-shaped microfiber coupler coated with polyvinyl alcohol film for highly sensitive humidity detection," Sens. Actuator A Phys. **285**, 628–636 (2019).
20. L. Zhou, Y. Yu, H. Huang, Y. Tao, K. Wen, G. Li, J. Yang, and Z. Zhang, "Salinity Sensing Characteristics Based on Optical Microfiber Coupler Interferometer," Photonics **7**(3), 77 (2020).
21. L. Zhou, Y. Yu, L. Cao, H. Huang, Y. Tao, Z. Zhang, J. Wang, J. Yang, and Z. Zhang, "Fabrication and Characterization of Seawater Temperature Sensor with Self-Calibration Based on Optical Microfiber Coupler Interferometer," Appl. Sci. **10**(17), 6018 (2020).
22. L. Cai and J. Li, "PDMS packaged microfiber knot resonator used for sensing longitudinal load change," J Phys Chem Solids **138**, 109268 (2020).
23. H. Wang, M. Liao, H. Xiao, X. Han, Y. Jiang, J. Tan, P. Zhang, J. Shao, Y. Tian, and J. Yang, "High sensitivity temperature sensor based on a PDMS-assisted bow-shaped fiber structure," Opt. Commun. **481**, 126536 (2021).
24. Z. Zhu, L. Liu, Z. Liu, Y. Zhang, and Y. Zhang, "Surface-plasmon-resonance-based optical-fiber temperature sensor with high sensitivity and high figure of merit," Opt. Lett. **42**(15), 2948–2951 (2017).
25. K. Li, T. Zhang, G. Liu, N. Zhang, M. Zhang, and L. Wei, "Ultrasensitive optical microfiber coupler based sensors operating near the turning point of effective group index difference," Appl. Phys. Lett. **109**(10), 101101 (2016).
26. L. Sun, Y. Semenova, Q. Wu, D. Liu, J. Yuan, X. Sang, B. Yan, K. Wang, C. Yu, and G. Farrell, "Investigation of humidity and temperature response of a silica gel coated microfiber coupler," IEEE Photonics J. **8**(6), 1–7 (2016).
27. L. Cao, Y. Yu, M. Xiao, J. Yang, X. Zhang, and Z. Meng, "High sensitivity conductivity-temperature-depth sensing based on an optical microfiber coupler combined fiber loop," Chin Opt Lett **18**(1), 011202 (2020).
28. Y. Bai, Y. Qi, Y. Dong, and S. Jian, "Highly sensitive temperature and pressure sensor based on Fabry–Perot interference," IEEE Photonics Technol. Lett. **28**(21), 2471–2474 (2016).
29. A. Leal-Junior, A. Frizera, C. Díaz, C. Marques, M. Ribeiro, and M. Pontes, "Material features based compensation technique for the temperature effects in a polymer diaphragm-based FBG pressure sensor," Opt. Express **26**(16), 20590 (2018).
30. A. Leal-Junior, C. Díaz, A. Frizera, C. Marques, M. Ribeiro, and M. Pontes, "Simultaneous measurement of pressure and temperature with a single FBG embedded in a polymer diaphragm," Opt Laser Technol. **112**, 77–84 (2019).